ACS Photonics

pubs.acs.org/journal/apchd5

Letter

Nonlinear Shift in Phonon-Polariton Dispersion on a SiC Surface

Shuta Kitade, Atsushi Yamada, Ikki Morichika, Kazuhiro Yabana, and Satoshi Ashihara*

Cite This: *ACS Photonics* 2021, 8, 152–157

Read Online

ACCESS | Metrics & More | Article Recommendations | Supporting Information

ABSTRACT: A nonlinear shift in the dispersion relation of a surface phonon-polariton (SPhP) is observed with grating-coupled pump–probe reflection spectroscopy. Upon excitation of an SPhP on a 4H-SiC surface, an instantaneous frequency shift of the SPhP mode at a constant wavevector is observed. This pump-induced frequency shift is equivalent to a nonlinear dispersion shift and to a Kerr-like nonlinear phase shift. The effective nonlinear index is evaluated to be orders of magnitude larger than the typical values of nonresonant dielectric responses. A nonlinear forced oscillator model aided by the first-principles calculations reproduce our observation and, furthermore, indicates that the primary origin is either the Born effective charge or the phonon anharmonicity depending on the frequency within the Reststrahlen band. The instantaneous shift is followed by a picosecond recovery, reflecting the energy relaxation and dissipation of the excited SPhP. This observed nonlinearity forms the basis of the self-phase modulation and four-wave mixing of SPhPs and paves the way toward nonlinear phonon-polaritonics.

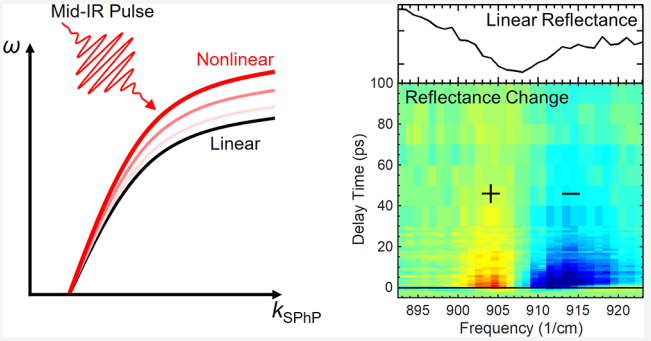

KEYWORDS: *surface phonon-polariton, nonlinear optics, infrared nanophotonics*

Surface phonon-polaritons (SPhPs) are localized modes where optical phonons are strongly coupled with infrared (IR) electromagnetic waves at dielectric surfaces.[1] Because of strong light–matter coupling, SPhPs exhibit a reduced phase and group velocities and, therefore, bring about a subwavelength localization and an electric-field enhancement, respectively. These properties make SPhPs promising for nanophotonic applications in the mid-IR range,[2−10] such as surface-enhanced spectroscopy,[3−6] thermal radiation control,[7,8] and strong-field phenomena.[9,10] To date, the linear properties of SPhPs, namely, the dispersion relation, have been intensively studied.[11−16]

Nonlinear responses of SPhPs may open a new avenue toward mid-IR nanophotonics, enabling self-phase modulation, four-wave mixing, and all-optical switching at a subwavelength scale. Regarding nonpolaritonic optical phonons, there have been reports on anharmonic oscillations,[17−19] parametric amplifications,[20] and the accompanying changes in material properties from these phenomena.[21−24] However, studies on the nonlinear responses of SPhPs are rather limited. Paarmann's group reported second harmonic generation from polar dielectric surfaces enhanced by SPhP excitations.[25−28] De Liberato's group developed a theoretical framework for $\chi^{(2)}$-processes of SPhPs[29] and $\chi^{(3)}$-processes of SPhPs.[30] To date, there has been no report on the experimental observation of the odd-order nonlinearity of SPhPs.

In this Letter, we experimentally observe a nonlinear shift in the dispersion relation of an SPhP on a 4H-SiC surface. By using IR pump–probe reflection spectroscopy combined with the grating coupling technique, we observe a pump-induced frequency shift in a SPhP mode that satisfies the grating coupling condition. This observation is naturally interpreted as a pump-induced change in the polariton dispersion and is equivalent to a Kerr-like nonlinear phase shift. The effective nonlinear index is evaluated to be orders of magnitude larger than the typical values of nonresonant electronic responses. A nonlinear forced-oscillator model aided by the first principle density functional theory (DFT) calculations reproduces the observed shift and indicates that the primary origin is either the Born effective charge or the phonon anharmonicity depending on the operation frequency. The model also predicts that the Kerr-like response is extraordinarily large at asymptotically high frequencies. These findings form the basis for nonlinear phonon-polaritonics, thereby opening a new avenue toward mid-IR nanophotonics.

Received: October 31, 2020
Published: December 28, 2020

METHODS

Strategy for Observing Nonlinear Shift in Dispersion. A SPhP on a dielectric surface exhibits a characteristic dispersion relation, where a derivative of the frequency ω with respect to the in-plane wavevector k decreases as ω approaches the asymptotically high frequencies.[1] If the dielectric surface is irradiated with intense light, the permittivity may be modified to renew the dispersion curve. A shift in the dispersion curve is observed either as a nonlinear phase shift at a constant frequency or as a frequency shift at a constant in-plane wavevector. To observe the latter, we exploit pump−probe reflection spectroscopy with the grating coupling technique.

Coupling with a Metal Grating. We use a metal grating to couple free-space IR light to a SPhP, as shown in Figure 1a.

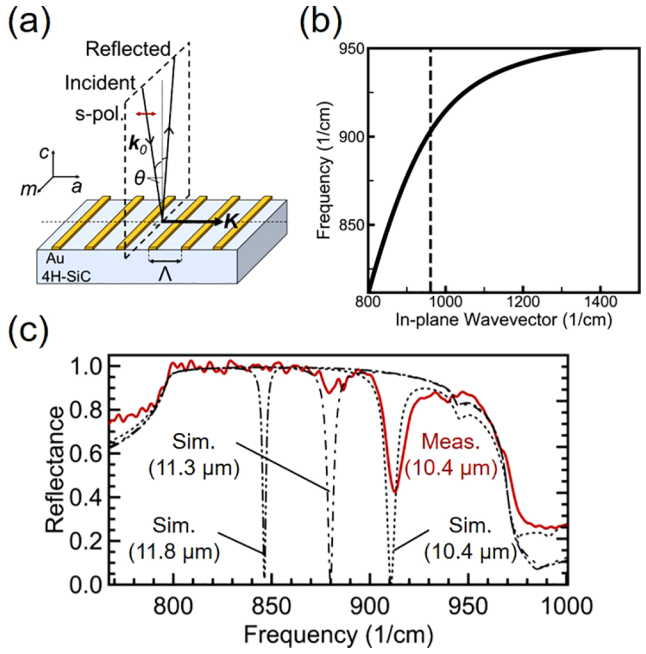

Figure 1. (a) Configuration of SPhP excitation with a metal grating. (b) Dispersion curve of a SPhP on a 4H-SiC (solid) and that of the incident free space light (the first-order diffraction, Λ = 10.4 μm, dashed). (c) Energy reflectance of a c-cut 4H-SiC surface patterned with a gold grating: simulated for different Λ's (black) and measured for Λ = 10.4 μm (red).

The grating coupling condition is expressed as $|\boldsymbol{k}_{\mathrm{SPhP}}| = \sqrt{(|\boldsymbol{k}_0|\sin\theta)^2 + (m|\boldsymbol{K}|)^2}$, where $\boldsymbol{k}_{\mathrm{SPhP}}$, $\boldsymbol{k}_0$, and $\boldsymbol{K}$ are the wavevectors of the SPhP, incident light, and metal grating, respectively; θ is the incident angle; and m is the integer. The magnitude of the grating wavevector is the reciprocal of the grating period Λ as $|\boldsymbol{K}| = 2\pi/\Lambda$. Gold gratings are fabricated on a 0.35 mm thick, semi-insulating c-cut 4H-SiC crystal by electron-beam lithography and a lift-off process. The gold wires are 3 μm wide and 200 nm high with a period of 10.4 μm.

Figure 1b shows the dispersion curve of an SPhP on a 4H-SiC (solid) and that of the first-order diffraction of the incident free space light for Λ = 10.4 μm (dashed). An efficient excitation of an SPhP is expected at the intersection where the grating coupling condition is satisfied. Figure 1c shows the energy reflectance values for the 4H-SiC surfaces patterned with gold gratings, simulated by using the finite-difference time-domain (FDTD) method and the permittivity of 4H-SiC reported in ref 31 (see Supporting Information I for details on the simulation method). Here, each grating consists of gold wires (a width of 3 μm and a height of 200 nm), arranged with a period Λ of 10.4, 11.3, and 11.9 μm. The reflectance is evaluated for the incident light (θ = 10°), which is linearly polarized perpendicular to the gold wires. For each grating period, we see a reflectance dip appearing in the Reststrahlen band at a frequency determined by the grating coupling condition.

A reflectance spectrum measured at an incident angle θ of 10° for a 4H-SiC surface with a grating (Λ = 10.4 μm) is shown as a red solid line in Figure 1c. Here, we use a Fourier transform IR spectrometer and a specular reflectance measurement unit. A BaF_2 wire grid polarizer is used to set the input polarization to be perpendicular to the gold wires. The reflection dip centered at 914 cm^{-1} with a fwhm of 11.5 cm^{-1} indicates efficient coupling into the SPhP mode. The slightly broader dip compared with the simulation result comes from the finite divergence angle of the incident light.

Pump−Probe Reflection Spectroscopy. Pump−probe reflection spectroscopy is performed by using IR pulses with a pulse energy of 400 nJ, a duration of 100 fs, a center frequency of 900 cm^{-1}, a fwhm bandwidth of 150 cm^{-1}, and a repetition rate of 1 kHz. The IR pulse is split into the pump and probe pulses by a wedged ZnSe window, and they spatially overlap with an off-axis parabolic mirror (an effective focal length of 3 in.) at the sample where the beam diameters are 280 μm (see Figure 2). Both the pump and the probe pulses are linearly

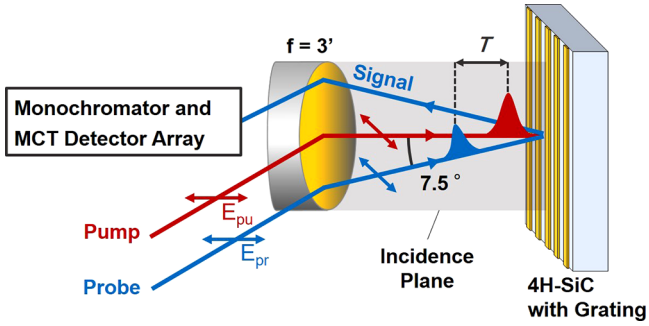

Figure 2. Schematic diagram showing the grating-coupled pump−probe reflection spectroscopy setup. Both the pump and probe pulses are linearly polarized perpendicular to the gold wires.

polarized perpendicular to the gold wires. The incidence angles of the pump and probe pulses are set to 0 and 7.5°, respectively, so that the probe geometry is similar to the linear reflection spectroscopy presented above. The spectrum of the reflected probe pulse is measured by a monochromator and HgCdTe (MCT) detector arrays. Here, the probe pulse monitors the pump-induced reflectance change at a variable delay time T.

Because the incidence angle of the probe pulse is different from that of the pump pulse by 7.5°, there is a difference in the excited SPhP frequency between the pump and probe pulses. This deviation, however, is estimated from the simulations shown in Figure 1a to be 2 cm^{-1}, much smaller than the resonance line width of 11.5 cm^{-1} (see the upper panel of Figure 3a). Thus, it is regarded as a degenerate pump−probe measurement. Nonetheless, the deviation of the excited SPhP frequency between the pump and probe pulses will not

https://dx.doi.org/10.1021/acsphotonics.0c01680
ACS Photonics 2021, 8, 152−157

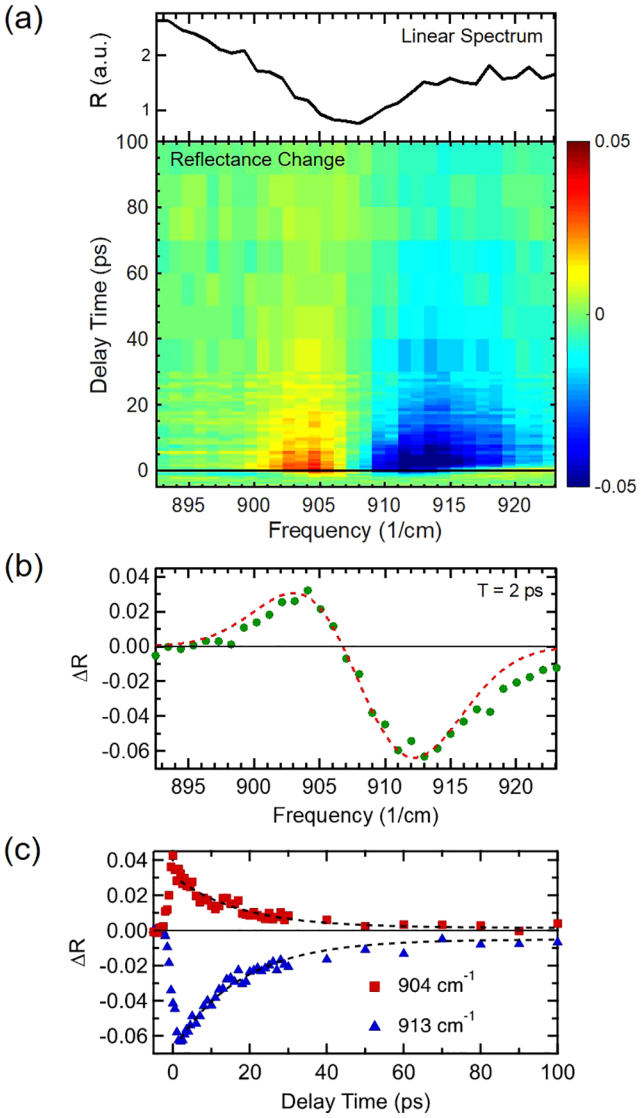

Figure 3. (a) Linear reflectance (upper panel) and the pump-induced reflectance change at various delay times (lower panel). (b) Pump-induced reflectance change ΔR at a 2 ps delay time. The dashed line represents a linear combination of two Gaussian functions fitted to the measured data. (c) The kinetics at probe frequencies of 904 (red squares) and 913 cm^{-1} (blue triangles). The dashed lines represent single exponential functions fitted to the data at delay times >2 ps.

significantly affect the observed signal, because it originates from local dielectric response whose resonance lies not at the operating frequency but at the TO phonon frequency (see Supporting Information III).

RESULTS

Figure 3a shows the transient reflectance change at different delay times, measured with a pump energy of 400 nJ (the electric field at the sample was 3.1 MV/cm). The upper panel shows the linear reflectance measured with the probe pulse, which exhibits a dip centered at 908 cm^{-1}. A slight deviation of the dip center compared with the one shown in Figure 1c results from a difference in the incidence angle. A pump-induced reflectance change at a 2 ps delay time is displayed in Figure 3b, and the kinetics at probe frequencies of 904 (red) and 913 cm^{-1} (blue) are displayed in Figure 3c. It is observed that positive and negative reflection changes are induced instantaneously upon excitation and decay with similar time constants.

Because the reflectance change has a bipolar nature and because the positive and negative signals exhibit identical kinetics, we can naturally interpret the observation as a blueshift of the reflectance dip. By fitting the reflectance change shown in Figure 3b with a linear combination of two Gaussian functions, we obtain center frequencies of 908.0 and 908.8 cm^{-1} and a common fwhm width of 11.5 cm^{-1}. This result indicates 0.8 cm^{-1} as a blueshift of the reflection dip.

By global fitting of the kinetics at varied probe frequencies with an exponential function, the recovery time of the pump-induced reflectance change is evaluated to be 17.1 ± 0.3 ps. Here, we naturally attribute the observed recovery of ~17 ps to the energy relaxation and/or dissipation of the excited SPhP mode. Note that the total dephasing time, evaluated from the simulated line width of the reflectance dip shown in Figure 2a, is 2 ps. Note also that the cooling of the gold wire is excluded as an origin for the observed recovery dynamics because the relevant time scales are much shorter (the electron−electron scattering is within 100 fs,[32] distribution of thermions throughout the wire is approximately 100 fs[33,34] and electron−lattice scattering is approximately 1 ps[35]) and that the cooling of 4H-SiC is excluded because the time scale of thermal dissipation is estimated to be ~1 ns at the earliest point.[36] The observed dynamics provide important insight into microscopic physics (anharmonic couplings to low-frequency phonons) that underlie the thermal conductivity of SPhPs,[37] which have excellent potential for nanoscale thermal conduction.[38]

DISCUSSION

Effective Nonlinear Refractive Index. Because a reflection dip appears at a frequency where the grating coupling condition is satisfied, the observed shift in the dip frequency should indicate a pump-induced change in the dispersion relation. Here, we recall that Boyd's group observed a shift in the incidence angle for a reflectance dip in the Kretschmann−Raether configuration upon strong excitation of a surface-plasmon polariton (SPP) on a Au surface.[39,40] They attributed the nonlinear shift to a change in the SPP's wavevector and in turn to the third-order nonlinear response of Au. In a similar fashion, our observed pump-induced change in the dispersion relation can be expressed either by a shift in the in-plane wavevector Δk^{SPhP} at a constant frequency ω_0 or a shift in the frequency $\Delta\omega$ at a constant in-plane wavevector $k_{\mathrm{SPhP}}(\omega_0)$, both of which are related by

$$\Delta k_{\mathrm{SPhP}} = \left(\frac{\mathrm{d}k_{\mathrm{SPhP}}}{\mathrm{d}\omega}\right)_{\omega=\omega_0} \Delta\omega \tag{1}$$

By introducing an effective refractive index n^{SPhP} as $k_{\mathrm{SPhP}} = (\omega/c)n^{\mathrm{SPhP}}$, we can relate Δk_{SPhP} with the effective index change $\Delta n^{\mathrm{SPhP}} = n_2^{\mathrm{SPhP}} I$ as

$$\Delta k_{\mathrm{SPhP}} = \frac{\omega}{c}\Delta n^{\mathrm{SPhP}} = \frac{\omega}{c} n_2^{\mathrm{SPhP}} I \tag{2}$$

where n_2^{SPhP} and I denote an effective nonlinear index and optical intensity, respectively. By using eqs 1 and 2 and the blueshift of 0.8 cm^{-1}, we obtain an effective nonlinear index n_2^{SPhP} of -2×10^{-13} cm^2/W. Compared with the nonlinear refractive index for a nonresonant electronic response

https://dx.doi.org/10.1021/acsphotonics.0c01680
ACS Photonics 2021, 8, 152−157

(typically ~ 10^{-16} cm^2/W), n_2^{SPhP} exhibits an opposite sign and a value that is orders of magnitude larger.

Theoretical Calculations of the Nonlinear Shift in the Dispersion Relation. An SPhP on the *c*-plane surface of 4H-SiC (uniaxial crystal) involves two electric field components, that are either parallel or perpendicular to the *c*-axis. Its dispersion curve is described as[41]

$$k_{SPhP}(\omega) = \frac{\omega}{c}\sqrt{\frac{\varepsilon_\perp\varepsilon_\parallel - \varepsilon_\parallel}{\varepsilon_\perp\varepsilon_\parallel - 1}} \quad (3)$$

where k_{SPhP} is the in-plane wavevector, c is the light velocity in vacuum, and $\varepsilon_\perp$ ($\varepsilon_\parallel$) is the relative permittivity for the electric field perpendicular (parallel) to the *c*-axis. We consider that the electric fields created by the grating coupling of the pump pulse induce changes in $\varepsilon_\perp$ and $\varepsilon_\parallel$ to modify the dispersion curve. For simplicity, we assume that a change in $\varepsilon_\perp$ ($\varepsilon_\parallel$) is induced by an electric field that is perpendicular (parallel) to the *c*-axis.

The nonlinear response of 4H-SiC in the Reststrahlen band can originate from the anharmonicity of the TO phonon potential,[17,18] the Born effective charge (or the phonon-electric field coupling), and the nonlinearity of the background (or nonresonant) dielectric response.[20] By considering these factors, we construct a nonlinear forced oscillator model and the corresponding equation of motion, which is described as eq S3.5 in Supporting Information III. The coefficients appearing in the equation are derived from the first-principles DFT calculations described in Supporting Information II.

We solve the equation of motion by the perturbative expansion procedure to calculate the nonlinear polarizations and the resulting permittivities of $\varepsilon_\perp$ and $\varepsilon_\parallel$. From the experimental pump electric field of 3.1 MV/cm and the simulated field distribution, the effective electric field that represents the spatially varying electric fields is estimated to be 3.4 (0.9) MV/cm for the component that is perpendicular (parallel) to the *c*-axis (see Supporting Information I). These effective values are used in eq S3.33 to calculate the modified permittivities of $\varepsilon_\perp$ and $\varepsilon_\parallel$ that renew the SPhP dispersion curve through eq 3.

Figure 4a shows the unmodified dispersion curve calculated with eq 3. The inset shows the modified (or nonlinear) dispersion curves, which are calculated by considering all/each of the possible origins. The dispersion curve shifts to a higher frequency by 0.3 cm^{-1} when all of the origins are taken into account, which is smaller, but comparable, to the experimentally observed value of 0.8 cm^{-1}. This discrepancy between the theoretical and experimental values of the frequency shift may come from the uncertainties in the evaluation of the effective electric fields and in the calculation of material's parameters (listed in Table S1 in Supporting Information II). The calculation also indicates that the major contributor to the dispersion shift is the Born effective charge at the measured frequency. The blueshift of the dispersion curve is viewed as a decrease in the in-plane wavevector at a constant frequency.

Figure 4b shows the shift of the in-plane wavevector, where all (each) of the possible origins are (is) taken into account. It is found that the shift in the wavevector is negative throughout the Reststrahlen band and is characterized by large values at frequencies close to the TO-phonon frequency (24 THz) and asymptotic values. The former is due to the more pronounced contribution from TO-phonon anharmonicity, and the latter is due to strong light−matter coupling. The corresponding effective nonlinear refractive index n_2^{SPhP} is calculated through eq 2 using the in-plane wavevector shift shown in Figure 4b. As can be seen from Figure 4c, n_2^{SPhP} also exhibits large negative values at frequencies close to the TO-phonon resonance and asymptotic values.

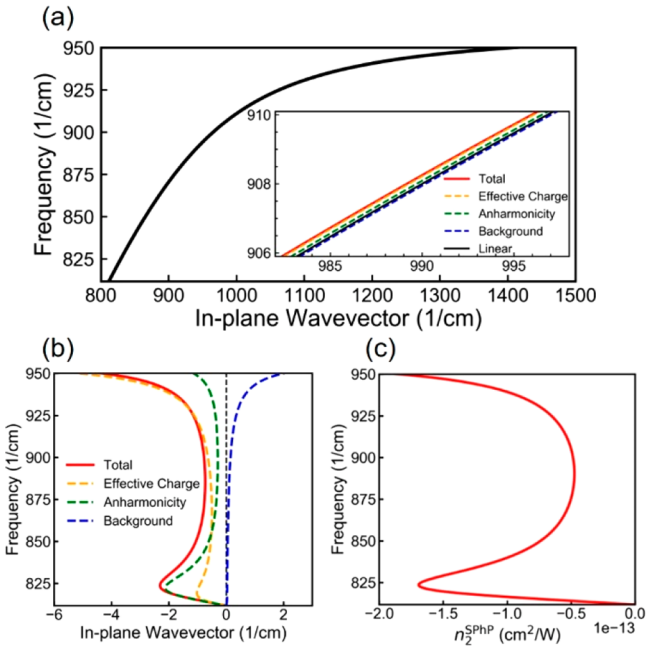

Figure 4. (a) Dispersion relation of the SPhP on a *c*-cut SiC. The inset shows the nonlinear dispersion curves that are calculated by considering all three origins (red), only the Born effective charge (yellow), only the TO-phonon anharmonicity (green), and only the background dielectric nonlinearity (blue). (b) Nonlinear shift of the in-plane wavevector, where all (each) of the possible origins are (is) taken into account. (c) Corresponding effective nonlinear index n_2^{SPhP}.

As presented above, the forced oscillator model not only explains the experimental observation but also predicts the nonlinear responses at various frequencies in the Reststrahlen band.

CONCLUSION

The nonlinear response of a SPhP on a 4H-SiC surface is observed by IR pump−probe reflection spectroscopy with the grating coupling technique. Upon resonant excitation of a SPhP mode, we observe an instantaneous blueshift of the SPhP mode that satisfies the grating coupling condition. The blueshift originates from the pump-induced modification of the polariton dispersion and can also be interpreted as the Kerr-like nonlinear phase shift. The effective nonlinear index is evaluated to be orders of magnitude larger than the typical values of nonresonant dielectric responses. The forced-oscillator model aided by the first-principles calculations quantitatively reproduces the observation and indicates that the primarily origin is either the Born effective charge (or the phonon-electric field coupling) or the phonon anharmonicity, depending on the operation frequency. The blueshift of the SPhP modes recovers at ~17 ps, which is interpreted as the energy relaxation/dissipation time of the SPhP mode. The observed nonlinearity forms the basis for the self-phase modulation and four-wave mixing of SPhPs, paving the way toward nonlinear mid-IR nanophotonics. Furthermore, the

https://dx.doi.org/10.1021/acsphotonics.0c01680
ACS Photonics 2021, 8, 152−157

revealed relaxation dynamics should also provide essential insight into the physics underlying the thermal conductivity at dielectric surfaces.

■ ASSOCIATED CONTENT

Supporting Information

The Supporting Information is available free of charge at https://pubs.acs.org/doi/10.1021/acsphotonics.0c01680.

Details of the FDTD simulations (S1), details of the first-principles DFT calculations of 4H-SiC (S2), details of the derivation of the third-order nonlinear susceptibility (S3), and details of the theoretical calculations of the nonlinear shift in dispersion on the *m*-plane surface (S4) (PDF)

■ AUTHOR INFORMATION

Corresponding Author

Satoshi Ashihara − *Institute of Industrial Science, The University of Tokyo, Tokyo 153-8505, Japan;* orcid.org/0000-0001-6697-2513; Phone: +81-3-5452-6136; Email: ashihara@iis.u-tokyo.ac.jp; Fax: +81-3-5452-6140

Authors

Shuta Kitade − *Institute of Industrial Science, The University of Tokyo, Tokyo 153-8505, Japan*

Atsushi Yamada − *Center for Computational Sciences, University of Tsukuba, Tsukuba 305-8577, Japan*

Ikki Morichika − *Institute of Industrial Science, The University of Tokyo, Tokyo 153-8505, Japan*

Kazuhiro Yabana − *Center for Computational Sciences, University of Tsukuba, Tsukuba 305-8577, Japan*

Complete contact information is available at: https://pubs.acs.org/10.1021/acsphotonics.0c01680

Notes

The authors declare no competing financial interest.

■ ACKNOWLEDGMENTS

K.Y. and S.A. acknowledge the support from the Ministry of Education, Culture, Sports, Science and Technology (Q-LEAP JPMXS0118068681). K.Y. acknowledges the support from Japan Science and Technology Agency (JST CREST JPMJCR16N5). S.A. acknowledges the support from the Japan Society for the Promotion of Science (18K19030, 20K20556) and Japan Science and Technology Agency (JST CREST JP20348765). The authors thank A. Sakurai (Institute for Molecular Science) and D. Okazaki (The University of Tokyo) for stimulating discussions.

■ REFERENCES

(1) Caldwell, J. D.; Lindsay, L.; Giannini, V.; Vurgaftman, I.; Reinecke, T. L.; Maier, S. A.; Glembocki, O. J. Low-Loss, Infrared and Terahertz Nanophotonics Using Surface Phonon Polaritons. *Nanophotonics* **2015**, *4*, 44−68.

(2) Stanley, R. Plasmonics in the Mid-Infrared. *Nat. Photonics* **2012**, *6*, 409−411.

(3) Neubrech, F.; Huck, C.; Weber, K.; Pucci, A.; Giessen, H. Surface-Enhanced Infrared Spectroscopy Using Resonant Nanoantennas. *Chem. Rev.* **2017**, *117*, 5110−5145.

(4) Kusa, F.; Morichika, I.; Takegami, A.; Ashihara, S. Enhanced Ultrafast Infrared Spectroscopy Using Coupled Nanoantenna Arrays. *Opt. Express* **2017**, *25*, 12896−12907.

(5) Morichika, I.; Murata, K.; Sakurai, A.; Ishii, K.; Ashihara, S. Molecular Ground-State Dissociation in the Condensed Phase Employing Plasmonic Field Enhancement of Chirped Mid-Infrared Pulses. *Nat. Commun.* **2019**, *10*, 3893.

(6) Kim, H. C.; Cheng, X. Surface Phonon Polaritons on SiC Substrate for Surface-Enhanced Infrared Absorption Spectroscopy. *J. Opt. Soc. Am. B* **2010**, *27*, 2393−2397.

(7) Greffet, J. J.; Carminati, R.; Joulain, K.; Mulet, J. P.; Mainguy, S.; Chen, Y. Coherent Emission of Light by Thermal Sources. *Nature* **2002**, *416*, 61−64.

(8) Ito, K.; Matsui, T.; Iizuka, H. Thermal Emission Control by Evanescent Wave Coupling Between Guided Mode of Resonant Grating and Surface Phonon Polariton on Silicon Carbide Plate. *Appl. Phys. Lett.* **2014**, *104*, No. 051127.

(9) Liu, H.; Guo, C.; Vampa, G.; Zhang, J. L.; Sarmiento, T.; Xiao, M.; Bucksbaum, P. H.; Vučković, J.; Fan, S.; Reis, D. A. Enhanced High-Harmonic Generation from an All-Dielectric Metasurface. *Nat. Phys.* **2018**, *14*, 1006−1010.

(10) Imasaka, K.; Kaji, T.; Shimura, T.; Ashihara, S. Antenna-Enhanced High Harmonic Generation in a Wide-Bandgap Semiconductor ZnO. *Opt. Express* **2018**, *26*, 21364−21374.

(11) Huber, A.; Ocelic, N.; Kazantsev, D.; Hillenbrand, R. Near-Field Imaging of Mid-Infrared Surface Phonon Polariton Propagation. *Appl. Phys. Lett.* **2005**, *87*, No. 081103.

(12) Huber, A. J.; Deutsch, B.; Novotny, L.; Hillenbrand, R. Focusing of Surface Phonon Polaritons. *Appl. Phys. Lett.* **2008**, *92*, 203104.

(13) Dai, S.; Fei, Z.; Ma, Q.; Rodin, A. S.; Wagner, M.; McLeod, A. S.; Liu, M. K.; Gannett, W.; Regan, W.; Watanabe, K.; Taniguchi, T.; Thiemens, M.; Dominguez, G.; Neto, A. H. C.; Zettl, A.; Keilmann, F.; Jarillo-Herrero, P.; Fogler, M. M.; Basov, D. N. Tunable Phonon Polaritons in Atomically Thin van der Waals Crystals of Boron Nitride. *Science* **2014**, *343*, 1125−1129.

(14) Shi, Z.; Bechtel, H. A.; Berweger, S.; Sun, Y.; Zeng, B.; Jin, C.; Chang, H.; Martin, M. C.; Raschke, M. B.; Wang, F. Amplitude- and Phase-Resolved Nanospectral Imaging of Phonon Polaritons in Hexagonal Boron Nitride. *ACS Photonics* **2015**, *2*, 790−796.

(15) Chen, D. Z. A.; Chen, G. Measurement of Silicon Dioxide Surface Phonon-Polariton Propagation Length by Attenuated Total Reflection. *Appl. Phys. Lett.* **2007**, *91*, 121906.

(16) Hafeli, A. K.; Rephaeli, E.; Fan, S.; Cahill, D. G.; Tiwald, T. E. Temperature Dependence of Surface Phonon Polaritons from a Quartz Grating. *J. Appl. Phys.* **2011**, *110*, No. 043517.

(17) Brennan, C. J.; Nelson, K. A. Direct Time-Resolved Measurement of Anharmonic Lattice Vibrations in Ferroelectric Crystals. *J. Chem. Phys.* **1997**, *107*, 9691−9694.

(18) Romero-Rochín, V. c.; Koehl, R. M.; Brennan, C. J.; Nelson, K. A. Anharmonic Phonon-Polariton Excitation through Impulsive Stimulated Raman Scattering and Detection through Wave Vector Overtone Spectroscopy: Theory and Comparison to Experiments on Lithium Tantalate. *J. Chem. Phys.* **1999**, *111*, 3559−3571.

(19) von Hoegen, A.; Mankowsky, R.; Fechner, M.; Först, M.; Cavalleri, A. Probing the Interatomic Potential of Solids with Strong-Field Nonlinear Phononics. *Nature* **2018**, *555*, 79−82.

(20) Cartella, A.; Nova, T. F.; Fechner, M.; Merlin, R.; Cavalleri, A. Parametric Amplification of Optical Phonons. *Proc. Natl. Acad. Sci. U. S. A.* **2018**, *115*, 12148−12151.

(21) Först, M.; Manzoni, C.; Kaiser, S.; Tomioka, Y.; Tokura, Y.; Merlin, R.; Cavalleri, A. Nonlinear Phononics as an Ultrafast Route to Lattice Control. *Nat. Phys.* **2011**, *7*, 854−856.

(22) Mitrano, M.; Cantaluppi, A.; Nicoletti, D.; Kaiser, S.; Perucchi, A.; Lupi, S.; Di Pietro, P.; Pontiroli, D.; Riccò, M.; Clark, S. R.; Jaksch, D.; Cavalleri, A. Possible Light-Induced Superconductivity in K3C60 at High Temperature. *Nature* **2016**, *530*, 461−464.

(23) Nova, T. F.; Cartella, A.; Cantaluppi, A.; Först, M.; Bossini, D.; Mikhaylovskiy, R. V.; Kimel, A. V.; Merlin, R.; Cavalleri, A. An Effective Magnetic Field from Optically Driven Phonons. *Nat. Phys.* **2017**, *13*, 132−136.

(24) Mankowsky, R.; von Hoegen, A.; Först, M.; Cavalleri, A. Ultrafast Reversal of the Ferroelectric Polarization. *Phys. Rev. Lett.* **2017**, *118*, 197601.
(25) Paarmann, A.; Razdolski, I.; Melnikov, A.; Gewinner, S.; Schöllkopf, W.; Wolf, M. Second Harmonic Generation Spectroscopy in the Reststrahl Band of SiC Using an Infrared Free-Electron Laser. *Appl. Phys. Lett.* **2015**, *107*, No. 081101.
(26) Razdolski, I.; Chen, Y.; Giles, A. J.; Gewinner, S.; Schöllkopf, W.; Hong, M.; Wolf, M.; Giannini, V.; Caldwell, J. D.; Maier, S. A.; Paarmann, A. Resonant Enhancement of Second-Harmonic Generation in the Mid-Infrared Using Localized Surface Phonon Polaritons in Subdiffractional Nanostructures. *Nano Lett.* **2016**, *16*, 6954−6959.
(27) Passler, N. C.; Razdolski, I.; Gewinner, S.; Schöllkopf, W.; Wolf, M.; Paarmann, A. Second-Harmonic Generation from Critically Coupled Surface Phonon Polaritons. *ACS Photonics* **2017**, *4*, 1048−1053.
(28) Razdolski, I.; Passler, N. C.; Gubbin, C. R.; Winta, C. J.; Cernansky, R.; Martini, F.; Politi, A.; Maier, S. A.; Wolf, M.; Paarmann, A.; De Liberato, S. Second Harmonic Generation from Strongly Coupled Localized and Propagating Phonon-Polariton Modes. *Phys. Rev. B: Condens. Matter Mater. Phys.* **2018**, *98*, 125425.
(29) Gubbin, C. R.; De Liberato, S. Theory of Nonlinear Polaritonics: $\chi^{(2)}$ Scattering on a β-SiC Surface. *ACS Photonics* **2017**, *4*, 1381−1388.
(30) Gubbin, C. R.; De Liberato, S. Theory of Four-Wave-Mixing in Phonon Polaritons. *ACS Photonics* **2018**, *5*, 284−288.
(31) Mutschke, H.; Anderson, A. C.; Clement, D.; Henning, T.; Peiter, G. Infrared properties of SiC particles. *Astron. Astrophys.* **1999**, *345*, 187−202.
(32) Wang, X.; Guillet, Y.; Selvakannan, P. R.; Remita, H.; Palpant, B. Broadband Spectral Signature of the Ultrafast Transient Optical Response of Gold Nanorods. *J. Phys. Chem. C* **2015**, *119*, 7416−7427.
(33) Sando, G. M.; Berry, A. D.; Campbell, P. M.; Baronavski, A. P.; Owrutsky, J. C. Surface Plasmon Dynamics of High-Aspect-Ratio Gold Nanorods. *Plasmonics* **2007**, *2*, 23−29.
(34) Park, S.; Pelton, M.; Liu, M.; Guyot-Sionnest, P.; Scherer, N. F. Ultrafast Resonant Dynamics of Surface Plasmons in Gold Nanorods. *J. Phys. Chem. C* **2007**, *111*, 116−123.
(35) Hartland, G. V. Optical Studies of Dynamics in Noble Metal Nanostructures. *Chem. Rev.* **2011**, *111*, 3858−3887.
(36) Siemens, M. E.; Li, Q.; Yang, R.; Nelson, K. A.; Anderson, E. H.; Murnane, M. M.; Kapteyn, H. C. Quasi-Ballistic Thermal Transport from Nanoscale Interfaces Observed Using Ultrafast Coherent soft X-Ray Beams. *Nat. Mater.* **2010**, *9*, 26−30.
(37) Teitelbaum, S. W.; Henighan, T.; Huang, Y.; Liu, H.; Jiang, M. P.; Zhu, D.; Chollet, M.; Sato, T.; Murray, É. D.; Fahy, S.; O'Mahony, S.; Bailey, T. P.; Uher, C.; Trigo, M.; Reis, D. A. Direct Measurement of Anharmonic Decay Channels of a Coherent Phonon. *Phys. Rev. Lett.* **2018**, *121*, 125901.
(38) Tranchant, L.; Hamamura, S.; Ordonez-Miranda, J.; Yabuki, T.; Vega-Flick, A.; Cervantes-Alvarez, F.; Alvarado-Gil, J. J.; Volz, S.; Miyazaki, K. Two-Dimensional Phonon Polariton Heat Transport. *Nano Lett.* **2019**, *19*, 6924−6930.
(39) De Leon, I.; Shi, Z.; Liapis, A. C.; Boyd, R. W. Measurement of the Complex Nonlinear Optical Response of a Surface Plasmon-Polariton. *Opt. Lett.* **2014**, *39*, 2274−2277.
(40) De Leon, I.; Sipe, J. E.; Boyd, R. W. Self-Phase-Modulation of Surface Plasmon Polaritons. *Phys. Rev. A: At., Mol., Opt. Phys.* **2014**, *89*, No. 013855.
(41) Borstel, G. F.; Falge, H. J. Surface Phonon-Polaritons. In *Electromagnetic Surface Modes*; Boardman, A. D., Ed.; Wiley: Chichester, 1975; p 219.

https://dx.doi.org/10.1021/acsphotonics.0c01680
ACS Photonics 2021, 8, 152−157